Investigation of the Richtmyer-Meshkov Instability with Double Perturbation Interface in Non-uniform Flows

Jing-song Bai,[1] Jin-hong Liu,[2] Tao Wang,[1] Li-yong Zou,[2] Ping Li,[1] Duo-wang Tan [2], and Cang-li Liu [2]

[1]*Institute of Fluid Physics, China Academy of Engineering Physics, Mianyang, Sichuan, P. R. China*

[2]*National Key Laboratory of Shock Wave and Detonation Physics (LSD), Institute of Fluid Physics, China Academy of Engineering Physics, Mianyang, Sichuan, P. R. China*

A non-uniform SF_6 gas flow initial condition has been actualized in the context of shock tube experiment for the Richtmyer-Meshkov instability study. Two kinds of amplitude have been used to design the membrane supports which initially materialize the gaseous interface. The visualizations of Air/SF_6 sinusoidal interfaces and shock wave propagations in the non-uniform field were obtained by Schlieren photography. Experiments are in very good agreement with simulations for the Air/SF_6 case, but due to the initial non-uniform effects, Sadot model and Zhang-Sohn theory are far beyond the experimental and calculation results.
PACS numbers: 47.40.Nm, 47.20.Ma

Richtmyer-Meshkov (RM) instability has been studied in many theoretical, numerical, and experimental works. Pure hydrodynamics RM experiments are mainly realized in shock tubes. In the case of the RM instability, the interface between the two gases is always unstable due to the vorticity production linked with the misalignment between the pressure and the density gradients when the shock wave passes through the interface. Afterwards the interface perturbations grow and develop into spikes and bubbles which can evolve into mushroom structures. The small perturbations initially presented on the interface will grow first linearly, then at later time, nonlinear development of the perturbations will take place and subsequent transition to turbulence will occur. The shock wave interaction with instable interface has gained much attention over the past decades, due to its importance in physics systems such as inertial confinement fusion (ICF) and astrophysical phenomena [1, 2]. As we all know that different initial conditions have a major effect on the development and evolution of the interface instability throughout the process. Numerous papers [3–7] stress the uncertainty about the initial conditions of the interface and it can induce more uncertainty in the use of experimental data to test numerical schemes. In all known horizontal or vertical shock tube experiments, the initial interfacial conditions are rarely accurately measured [5,8] but often backwards estimated. Recently, a novel method to produce an accurately profiled initial interface has been developed to study the instability of a gaseous interface impulsively accelerated in a shock tube. [9] As a consequence, experiments that are more suited to both theoretical and numerical studies are needed.

In those papers published, whether experimental or numerical simulation studies interface instability, the initial flows are almost seen as a uniform flow field. However, we are well aware that the initial flow state could produce to a certain extent effect on development and evolution of the interface instability. Thus, the aim of the present letter is to investigate the influence of non-uniform flow initial conditions on the interface instability. The experiments are performed in the LSD's horizontal shock tube which is 5 m long, and 20×10 cm^2 rectangular cross section. It is coupled with a high speed Schlieren photography (the time between two consecutive frames is 100 micro s) which allows a 2D visualization of the interface. We chose the air and SF_6 gases, and hope the SF_6 gas constitutes the initial non-uniform flow field. The incident shock wave mach number is 1.27 in air. The air shock wave through the air and SF_6 interface, and enter into the SF_6 gas non-uniform flow field. Meanwhile we set two different kinds of initial

perturbations with the same wavelength and different amplitude on the interface, the purpose is to observe the impact of the non-uniform flow field on the development and evolution of perturbation. How to achieve non-uniform flow field and determine the initial state parameters of non-uniform flow field are the first to be considered before the experiment, as it may directly impact on interface instability. First of all, for obtaining an initial non-uniform SF_6 gas flow field, the simplest and natural way is that two holes with diameter Φ10 mm are opened at the bottom and top of shock tube respectively, and the SF_6 gas is injected into the shock tube from the lower hole and left from the upper hole. In order to maintain a constant pressure of SF_6 gas flow field, the gas flow speed is very slow, about 0.417 cm/s. When the SF_6 gas flow speed stabilizes more than 20 minutes later, we begin to experiment. As the gas diffusion effect will make a larger proportion of SF_6 gas in the lower part of shock tube, it can form naturally the initial non-uniform flow field. The state of SF_6 gas before experiment is that the concentration is larger with higher density at the lower part of shock tube, and the concentration is smaller with lower density at the upper part of shock tube. The pressure of initial non-uniform flow field is one atmospheric, and the initial spatial distribution of density is difficult to be measured in vertical direction and not known. In the experiment, we mainly measured the SF_6 gas concentrations at the entrance (bottom) and exit (top), they are 0.95 and 0.71 respectively. Therefore we need to determine the initial distribution of density in the non-uniform flow field with the help of numerical simulation and experimental results, for reproducing the whole experimental process and understanding the impact of non-uniform flow field on the development and evolution of perturbations. This work has an important significance on the setting of initial conditions for experimental study of interface instability, analysis of experimental phenomenon and results. Air/SF_6 interface for dual-mode sinusoidal perturbation is that the wavelength is 0.05m, wave number $\omega = 2\pi/\lambda$, and the amplitudes are $A_1 = 5.0 \times 10^{-3}$ m and $A_2 = 7.5 \times 10^{-3}$ m respectively, the perturbation function is $x = A_1 \sin(\omega y)$ when $0.0 \le y < 0.0875$ m and $x = A_2 \sin(\omega y)$ when $0.0875 < y \le 0.2$ m. The size of Schlieren photography observation test window is 0.212×0.2 m^2 in the x-y plane in our experiment. The initial structure diagram is shown in Figure 1, the initial shock front is located at $x = 5.56 \times 10^{-3}$ m, the equilibrium position of perturbation is at $x = 0.016$m, the range of observation test window is [0.038m, 0.25m] corresponding to experiment in the x

direction. For avoiding the influence of the membrane, a thin nitro cellulosic membrane (about ~1μm thickness) is constructed. Table I summarizes the properties of air and SF$_6$ gas in the present experiment at 1 atmospheric pressure and 20℃.

TABLE I Properties of air and SF$_6$ gas.

Gas	Density (kg/m^3)	Specific heat ratio	Kinematic viscosity (10^{-6}m^2/s)	Prandtl number	Diffusion coefficient in air (cm^2/s)
Air	1.29	1.40	15.7	0.71	0.204
SF$_6$	5.34	1.09	2.47	0.90	0.097

This letter presents the numerical simulation investigation of the experiment. Based on the multi-viscous-fluid piecewise parabolic method, [10] the Vreman [11] subgrid eddy viscosity model is employed to the Navier-Stokes equations. Two- and three- dimensional large eddy simulation code MVFT2D (2D multi-viscous flow and turbulent) and MVFT3D for the multi-viscosity-fluid and turbulence resulting from the fluid interface instability are developed. The flow equations are given by

$$\begin{cases} \dfrac{\partial \bar{\rho}}{\partial t} + \dfrac{\partial \bar{\rho}\tilde{u}_j}{\partial x_j} = 0 \\[2mm] \dfrac{\partial \bar{\rho}\tilde{u}_i}{\partial t} + \dfrac{\partial \bar{\rho}\tilde{u}_j\tilde{u}_i}{\partial x_j} + \dfrac{\partial \bar{p}}{\partial x_i} = \dfrac{\partial(\bar{\sigma}_{ij}+\tau_{ij})}{\partial x_j} \\[2mm] \dfrac{\partial \bar{\rho}\bar{E}}{\partial t} + \dfrac{\partial \left(\bar{\rho}\tilde{u}_j\bar{E}+\bar{p}\tilde{u}_j\right)}{\partial x_j} = -\dfrac{\partial(\bar{q}_j+Q_j)}{\partial x_j} + \dfrac{\partial\left(\tilde{u}_i(\bar{\sigma}_{ij}+\tau_{ij})\right)}{\partial x_j} \\[2mm] \dfrac{\partial \bar{Y}^{(s)}}{\partial t} + \tilde{u}_j\dfrac{\partial \bar{Y}^{(s)}}{\partial x_j} = \dfrac{\partial}{\partial x_j}\left(\tilde{D}\dfrac{\partial \bar{Y}^{(s)}}{\partial x_j}\right) \quad s=1,2,\cdots,N-1 \end{cases} \quad (1)$$

$\bar{\sigma}_{ij} = \mu_t(\partial\tilde{u}_i/\partial x_j + \partial\tilde{u}_j/\partial x_i - 2/3\delta_{ij}(\partial\tilde{u}_k/\partial x_k))$ is the viscous stress tensor, $\tau_{ij} = \rho(\widetilde{u_iu_j}-\tilde{u}_i\tilde{u}_j)$ is the subgrid scale (SGS) stress tensor, $\bar{q}_j + Q_j$ is the energy flux of unit time and space, $\bar{q}_j = -\lambda_l\partial\bar{T}/\partial x_j$, $Q_j = -\lambda_t\partial\bar{T}/\partial x_j$, $\lambda_l = \mu_l c_p/p_{r,l}$, $\lambda_t = \mu_t c_p/p_{r,t}$, $\tilde{D} = \bar{D}_l + D_t$, $S_{c,t} = \mu_t/D_t\bar{\rho}$. μ_l is the fluid viscosity, T is the temperature, λ_l is the efficient heat-transfer coefficient, c_p is the specific heat of fluid, $p_{r,l}$ is the Prandtl number, $\bar{D}_l$ is the diffusion coefficient and D_t is the turbulent diffusion coefficient. Operator splitting technique is used to decompose the physical problems, described by equations (1), into three sub-processes, i.e. the computation of inviscid flux, viscous flux and heat flux. The equations (1) can be decomposed into two equations as follows

$$\begin{cases} \dfrac{\partial \bar{\rho}}{\partial t} + \dfrac{\partial \bar{\rho}\tilde{u}_j}{\partial x_j} = 0 \\[2mm] \dfrac{\partial \bar{\rho}\tilde{u}_i}{\partial t} + \dfrac{\partial \bar{\rho}\tilde{u}_j\tilde{u}_i}{\partial x_j} + \dfrac{\partial \bar{p}}{\partial x_i} = 0 \\[2mm] \dfrac{\partial \bar{\rho}\bar{E}}{\partial t} + \dfrac{\partial \left(\bar{\rho}\tilde{u}_j\bar{E}+\bar{p}\tilde{u}_j\right)}{\partial x_j} = 0 \\[2mm] \dfrac{\partial \bar{Y}^{(s)}}{\partial t} + \tilde{u}_j\dfrac{\partial \bar{Y}^{(s)}}{\partial x_j} = 0 \quad s=1,2,\cdots,N-1 \end{cases} \quad (2)$$

$$\begin{cases} \dfrac{\partial \bar{\rho}}{\partial t} = 0 \\[2mm] \dfrac{\partial \bar{\rho}\tilde{u}_i}{\partial t} = \dfrac{\partial(\bar{\sigma}_{ij}+\tau_{ij})}{\partial x_j} \\[2mm] \dfrac{\partial \bar{\rho}\bar{E}}{\partial t} = -\dfrac{\partial(\bar{q}_j+Q_j)}{\partial x_j} + \dfrac{\partial\left(\tilde{u}_i(\bar{\sigma}_{ij}+\tau_{ij})\right)}{\partial x_j} \\[2mm] \dfrac{\partial \bar{Y}^{(s)}}{\partial t} = \dfrac{\partial}{\partial x_j}\left(\tilde{D}\dfrac{\partial \bar{Y}^{(s)}}{\partial x_j}\right) \quad s=1,2,\cdots,N-1 \end{cases} \quad (3)$$

For the inviscid flux, the 3D problem can be simplified into three 1D problems by dimension splitting technique. For the 1D problem, we apply two-step Lagrange/Remap algorithm to solve the equations, and a time step calculation can be divided into four steps: ① the piecewise parabolic interpolation of physical quantities, ②solving Riemann problems approximately, ③ marching of Lagrange equations, and ④ Remapping the physical quantities to stationary Euler meshes. More information can be obtained in the author's literature. [12] For the viscous flux and heat flux, they are calculated by utilizing second-order spatial center difference and two-step Rung-Kutta time marching. The Vreman SGS turbulent model is applied [11]

$$\mu_t = C_V\rho\sqrt{\dfrac{II_\beta}{\bar{\alpha}_{ij}\bar{\alpha}_{ij}}} \quad (4)$$

with $\bar{\alpha}_{ij} = \partial\bar{u}_j/\partial x_i$,
$II_\beta = \beta_{11}\beta_{22} - \beta_{12}^2 + \beta_{11}\beta_{33} - \beta_{13}^2 + \beta_{22}\beta_{33} - \beta_{23}^2$,
$\beta_{ij} = \sum_{m=1}^{3}\Delta_m^2\bar{\alpha}_{mi}\bar{\alpha}_{mj}$. The model constant C_V is related to the Smagorinsky constant C_S by $C_V \approx 2.5C_S^2$ ($C_V = 0.07$ in this paper).

For the initial non-uniform SF$_6$ gas flow field, numerical simulation is used to approximately describe the dissipative transition layer. [13] In the dissipative transition layer, SF$_6$ gas density is calculated by Gaussian function:

$$\rho(y) = \rho_{SF_6}e^{-((y-y_c)^2/\delta^2)} \quad (5)$$

where $y_c=0$, and $\delta=0.3729$m. The calculating region is [-0.02m, 0.25m]×[0.0m, 0.2m], and it is discretized into 540×400 grids. Sample images from the experiment and the corresponding numerical results are shown in Figure 2. These images have been chosen because they can illustrate some salient features of the experiment. By using the Schlieren photography, we obtained two-dimensional flow field schlieren diagram from t=0.2ms to 2.0ms at intervals of 0.2ms, and they are shown in the right side of Figure 2 (a) - Figure 2 (j) (The black vertical strip in the each figure is the transparent glass support structure). From the experimental results in Figure 2 (a) - Figure 2 (j), we can see that, due to the non-uniform flow field of SF$_6$ gas, the density distribution changes from high to low along the shock tube vertically, and this results in the propagating velocity of shock wave in the upper part of shock tube faster than in the bottom of shock tube, and forms an oblique shock wave front. The calculating images of MVFT2D are shown in the left side of Figure 2 (a) - Figure 2 (j) (the white vertical dashed lines denote the supporting frames). Figure 2 shows that the calculated development of the interface shape, location, and oblique shock wave propagating features are consistent with the experimental results. The main difference between calculation and experiment is that the experimental schlieren shock tube map is the integral results along the thickness direction, but the calculated result is only a two-dimensional section. If we do not take into account the non-uniformity of SF$_6$ gas in the calculation, then the calculated results of the interface shape, location, and oblique

shock propagating characteristics will be quite different from experimental results. Figure 3 shows two kinds of calculated results and experimental images at 1.0ms, the difference is clear and will be discussed in the following part. Turbulence is a highly complex three-dimensional unsteady state, with a rotating irregular flow. The physical parameters of turbulence such as speed, pressure, temperature and so on change randomly over time and space, and can be regarded as random distribution, the turbulent flow can also be superimposed by a variety of different scales vortex. The above calculation is only in two-dimensional x-y plane shock tube, and did not consider the dissipation in z direction. Two-dimensional calculation results may be stronger, so we also carried out three-dimensional numerical simulation. The thickness of three-dimensional model in z direction is 5cm, the total calculating grids are $540\times400\times100$. Figure 4 shows the comparison between two and three-dimensional calculating results, it can be seen that both the calculating shape and location of the interface is almost exactly same, and the difference of physics characteristics in the flow are very small. So we think the RM instability in this experiment has not yet fully developed to the turbulent state.

The degree of influence can be described by the two measureable properties in our shock tube experiments. The first is to accurately catch the two kinds of initial sinusoidal perturbations with same wavelength and different amplitude of the gaseous interface, and the second is to exactly capture the front of shock wave in the non-uniform flow field. These two properties become the keys in our experiments. Figure 5 shows the locations of bubble and spike, and three shock front line observation. In Figure 5, B1-S1 correspond to the position of peak and trough of the initial small perturbation, and B3-S3 correspond to the position of peak and trough of the initial large perturbation, while the positions of three observed shock front are Line I 17.26cm, Line II 9.82cm, and Line III 2.78cm respectively. Figure 6 shows the location of three test lines at different times, including experimental and calculated results. When the time is greater than 1.0ms, the shock front has spread out the testing window, and the figure did not give comparative data. From the comparison of the results in Figure 6, we can see that the difference between calculated and experimental shock-front position along the Line I is about 5% before 0.4ms, afterwards the difference is almost same. Along the Line II and Line III, shock-front location of calculation and experiment is almost perfectly matching in early times, but the difference is about 3% after 0.8ms. This difference may be due to the initial calculation of density distribution for non-uniform flow field using Gaussian function, it is just an approximation of the real situation. This approximation describes the flow field characteristics and a smaller difference with the practice is acceptable. Figure 7 shows the comparison between the B1-S1 and B3-S3 perturbation amplitude histories of experiment, numerical computing, Sadot model and the theory of Zhang-Sohn, in which the bar denotes the experimental error about $\pm10\%$. From Figure 7 we can see that, for the two different kinds of perturbation, the difference between numerical and experimental values were within 10%, while the results of Sadot model for B1-S1 amplitude is closer to experimental and computational results, the results of Sadot model for B3-S3, as well as Zhang-Sohn theory for the both is far beyond the experimental and computational results. In order to analyze the effect of initial uniform and non-uniform flow fields on the interface instability, Figure 8 shows the calculated history of two kinds of perturbation amplitude for initial uniform and non-uniform flow field. As it can be seen that

there are two kinds of differences: for uniform flow field, when t>0 the perturbation amplitude of B3-S3 is always greater than the perturbation amplitude of B1-S1. But for non-uniform flow field, at $0<t\leq1.3$ms the perturbation amplitude of B3-S3 is greater than the perturbation amplitude of B1-S1, while at t> 1.3ms the opposite results appeared, the perturbation amplitude of B1-S1 is greater than the perturbation amplitude of B3-S3. This interesting phenomenon shows that for the RM instability, in addition to the initial conditions of perturbation interface, the flow field non-uniformity also has a significant effect on the interface instability.

In summary, an initial condition of non-uniform SF_6 gas flow has been actualized in the context of shock tube experiment for the RM instability study. By using Schlieren photography, the Air/SF_6 sinusoidal interfaces and shock wave propagations in the non-uniform field were obtained. By the numerical simulation tool, we determined the initial density distribution of non-uniform flow field, and reproduced the whole experimental process. At the same time, the differences of the initial non-uniform or uniform flow to the RM instability were analyzed, numerical and experiment results are compared to the Sadot model and Zhang-Sohn theory. This work illuminated that besides owning the identity of initial interface condition, the initial non-uniform flow would have a significant effect on the RM instability.
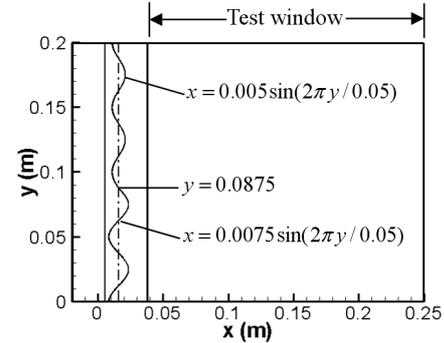
Figure 1 Initial structure diagram in the shock tube.

(a) t=0.2ms   (b) t=0.4ms

(c) t=0.6ms   (d) t=0.8ms

(e) t=1.0ms   (f) t=1.2ms

(g) t=1.4ms   (h) t=1.6ms

3

(i) t=1.8ms   (j) t=2.0ms
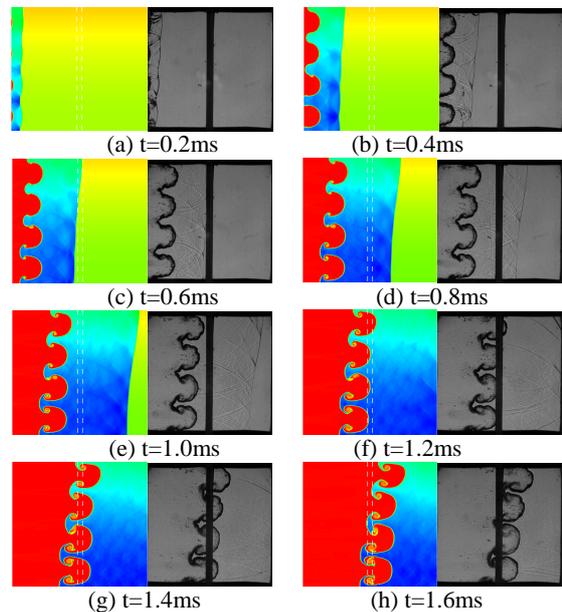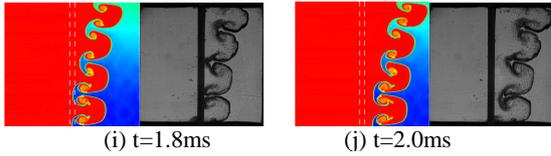
Figure 2 (Color online) Schlieren photography pictures and numerical simulation results by MVFT2D at a certain time (The sizes of the pictures are ones of the test window [0.038m, 0.25m]×[0.0m, 0.2m]).

(a)   (b)
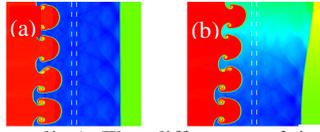
Figure 3 (Color online) The difference of interface shape, location and shock front at t=1.0ms between the initial uniform and non-uniform flow (The sizes of the pictures are same as Figure 2). (a) Initial uniform flow (b) Initial non-uniform flow

(a) t=1.0ms   (b) t=2.0ms
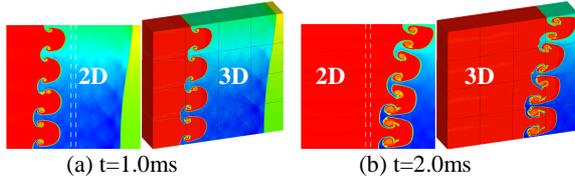
Figure 4 (Color online) Comparisons of the MVFT2D's and MVFT3D's results at two times (The sizes of the pictures are same as Figure 2).
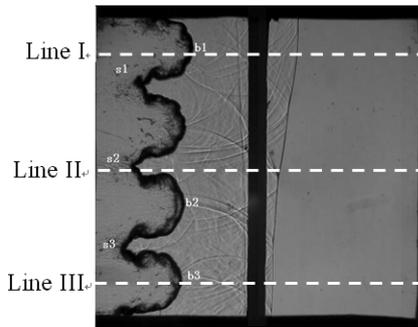
Figure 5 Bubble and spike locations in test window, as well as three shock front line positions.
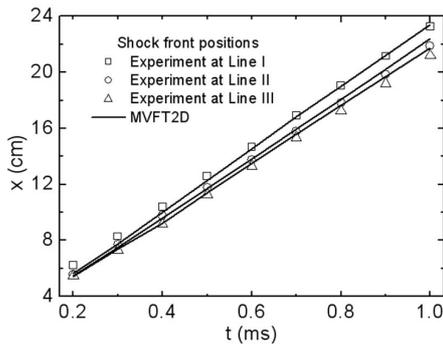
Figure 6 Shock front locations of the experiment and calculated results on the three test lines at different time.

(a) B1-S1

(b) B3-S3
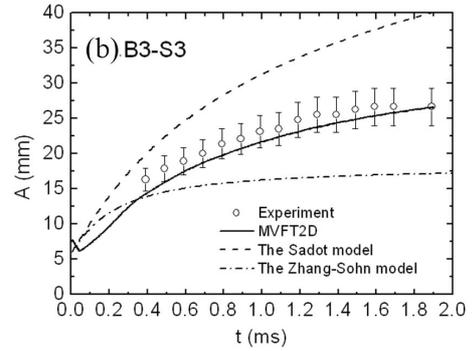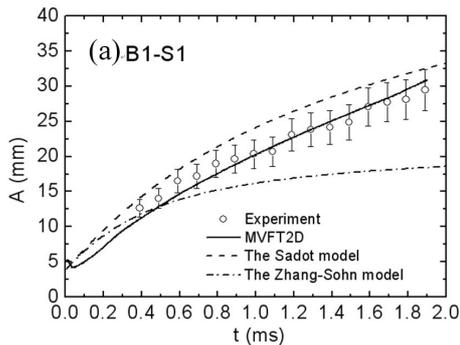
Figure 7 Perturbation amplitudes history of the experiment, numerical computing, and comparison with the Sadot model and Zhang-Sohn theory, B1-S1 corresponds to the small perturbation amplitude, and B3-S3 corresponds to the large one. (The error bars of this visual measurement are equal to ±10%)
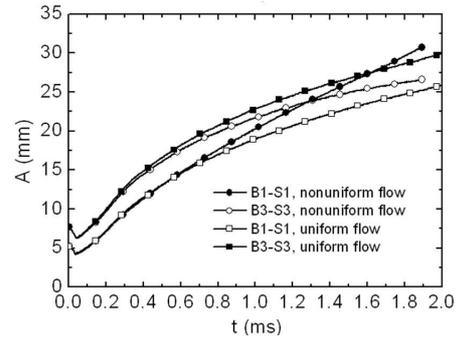
Figure 8 Perturbation amplitude history calculations of the initial uniform and non- uniform flow in RM instability.

[1] Puranik P B, Oakley J G, Anderson MH, Bonazza R, Shock Waves **13**, 413 (2004).

[2] D Arnett, J. Suppl. **127,** 213 (2000)

[3] J. Grove, R. Holmes, D. Sharp, Y. Yang, and Q. Zhang, Phys. Rev. Lett. **71**, 3473 (1993).

[4] K. Mikaelian, Phys. Rev. Lett. **71**, 2903 (1993).

[5] P. Puranik, J. Oakley, M. Anderson, and R. Bonazza, Shock Waves **13**, 413 (2004).

[6] D. Hill, C. Pantano, and D. Pullin, J. Fluid Mech. **557**, 29 (2006).

[7] K. Mikaelian, Phys. Rev. Lett. **80**, 508 (1998).

[8] E. Meshkov, Fluid Dyn. **4**, 101 (1972).

[9] C. Mariani, M. Vandenboomgaerde, G. Jourdan, D. Souffland, and L. Houas, Phys. Rev. Lett. **100**, 254503 (2008).

[10] J S Bai, P Li, T Wang, B Xie, M Zhong, S H Chen, Explosion and Shock Waves **27**, 515 (2007).

[11] W Vreman, Phys. fluids **16**, 3670 (2004).

[12] J S Bai, P Li, L Y Zou, T Wang, Chinese Journal of Theoretical and Applied Mechanics **40**, 464 (2008).

[13] S Gupta, S Zhang, Laser and Particle Beams **21,** 403(2003).